

## Heterogeneous Cadherin Expression and Multicellular Aggregate Dynamics in Ovarian Cancer Dissemination



Yuliya Klymenko<sup>\*†</sup>, Jeffrey Johnson<sup>†</sup>,  
Brandi Bos<sup>\*†</sup>, Rachel Lombard<sup>†</sup>, Leigh Campbell<sup>†</sup>,  
Elizabeth Loughran<sup>†,‡</sup> and M. Sharon Stack<sup>\*†,‡</sup>

<sup>\*</sup>Dept. of Biological Sciences, University of Notre Dame, South Bend, IN, 46617; <sup>†</sup>Harper Cancer Research Institute, University of Notre Dame, South Bend, IN, 46617; <sup>‡</sup>Dept. of Chemistry and Biochemistry, University of Notre Dame, South Bend, IN, 46617

### Abstract

Epithelial ovarian carcinoma spreads via shedding of cells and multicellular aggregates (MCAs) from the primary tumor into peritoneal cavity, with subsequent intraperitoneal tumor cell:mesothelial cell adhesion as a key early event in metastatic seeding. Evaluation of human tumor extracts and tissues confirms that well-differentiated ovarian tumors express abundant E-cadherin (Ecad), whereas advanced lesions exhibit upregulated N-cadherin (Ncad). Two expression patterns are observed: “mixed cadherin,” in which distinct cells within the same tumor express either E- or Ncad, and “hybrid cadherin,” wherein single tumor cell(s) simultaneously expresses both cadherins. We demonstrate striking cadherin-dependent differences in cell-cell interactions, MCA formation, and aggregate ultrastructure. Mesenchymal-type Ncad<sup>+</sup> cells formed stable, highly cohesive solid spheroids, whereas Ecad<sup>+</sup> epithelial-type cells generated loosely adhesive cell clusters covered by uniform microvilli. Generation of “mixed cadherin” MCAs using fluorescently tagged cell populations revealed preferential sorting into cadherin-dependent clusters, whereas mixing of cell lines with common cadherin profiles generated homogeneous aggregates. Recapitulation of the “hybrid cadherin” Ecad<sup>+</sup>/Ncad<sup>+</sup> phenotype, via insertion of the *CDH2* gene into Ecad<sup>+</sup> cells, resulted in the ability to form heterogeneous clusters with Ncad<sup>+</sup> cells, significantly enhanced adhesion to organotypic mesomimetic cultures and peritoneal explants, and increased both migration and matrix invasion. Alternatively, insertion of *CDH1* gene into Ncad<sup>+</sup> cells greatly reduced cell-to-collagen, cell-to-mesothelium, and cell-to-peritoneum adhesion. Acquisition of the hybrid cadherin phenotype resulted in altered MCA surface morphology with increased surface projections and increased cell proliferation. Overall, these findings support the hypothesis that MCA cadherin composition impacts intraperitoneal cell and MCA dynamics and thereby affects ultimate metastatic success.

*Neoplasia* (2017) 19, 549–563

Abbreviations: 3D, three-dimensional; BSA, bovine serum albumin; CMFDA, green 5-chloromethylfluorescein diacetate; CMTPX, 4-([4-(chloromethyl)phenyl]carbonyl)amino)-2-(1,2,2,4,8,10,10,11-octamethyl-10,11-dihydro-2H-pyrano[3,2-g:5,6-g']diquinolin-1-ium-6-yl)benzoate; Ecad, E-cadherin; ECM, extra-cellular matrix; EGF, epidermal growth factor; eGFP, enhanced green fluorescent protein; EMT, epithelial-to-mesenchymal transition; EOC, epithelial ovarian carcinoma; FBS, fetal bovine serum; hGAPDH, housekeeping glyceraldehyde 3-phosphate dehydrogenase; GFP, green fluorescent protein; MCA, multicellular aggregate; MEM, minimal essential medium; MET, mesenchymal-to-epithelial transition; Ncad, N-cadherin; NEAA, non-essential amino acids; PBS, phosphate-buffered saline; qPCR, quantitative polymerase chain reaction; RFP, red fluorescent protein; RTCI, rat tail collagen type

I; SEM, scanning electron microscopy; SFM, serum-free medium; TEM, transmission electron microscopy; TMA, tissue microarray.

Address all correspondence to: M. Sharon Stack, University of Notre Dame, 1234 Notre Dame Ave., A200 Harper Hall, South Bend, IN 46617.

E-mail: [sstack@nd.edu](mailto:sstack@nd.edu)

Received 19 November 2016; Revised 30 March 2017; Accepted 3 April 2017

© 2017 The Authors. Published by Elsevier Inc. on behalf of Neoplasia Press, Inc. This is an open access article under the CC BY-NC-ND license (<http://creativecommons.org/licenses/by-nc-nd/4.0/>).

1476-5586

<http://dx.doi.org/10.1016/j.neo.2017.04.002>

## Introduction

Epithelial ovarian carcinoma (EOC) is the fifth leading cause of cancer-related death among women and the most lethal of all gynecological malignancies with 22,280 new cases and 14,240 deaths estimated in the United States in 2016 [1]. The location and size of the ovaries and fallopian tubes, relatively nonspecific symptoms, and absence of reliable screening methods make EOC difficult to detect in early stages and worsen the survival prognosis. The vast majority of women are diagnosed with stage III to IV disease with involvement of distant organs and lymph nodes, resulting in a 5-year relative survival rate of about 25%. In contrast, women with localized cancer whose lesions are limited to primary tumor site have a 95% 5-year survival [2]. Notably, most patients initially respond very well to chemotherapy but later relapse with more advanced, multidrug-resistant metastatic disease [3,4]. Therefore, it is crucial to gain understanding of the mechanisms involved in metastatic success in order to develop novel therapeutic approaches that could improve long-term survival.

In contrast to most other tumors that spread predominantly through lymph or bloodstream, ovarian cancer disseminates mainly via direct extension of cancer cells from the primary tumor into the intra-abdominal cavity, wherein they survive and travel as single cells and multicellular aggregates (MCAs) with the peritoneal fluid flow, subsequently adhering to peritoneal tissues, anchoring in the submesothelial matrix, and proliferating to form secondary lesions [5,6]. Hematogenous metastasis has also been described [7,8]. Free-floating EOC aggregates are abundant in the peritoneal cavity; however, the number, size, and integrity of aggregates vary considerably [9,10]. Although free-floating single cells and MCAs were previously considered as nonadhesive units that do not contribute to metastatic progression, it is now generally accepted that MCAs are indeed metastatically competent and can actively adhere to peritoneal mesothelium and submesothelial extracellular matrix [11]. Nevertheless, most patient-derived MCAs that adhere to and disperse on extracellular matrix components (such as collagen type I) and mesothelial cell layers display limited invasion, suggesting the existence of a subpopulation of MCAs with enhanced metastatic properties [12]. Due to difficulties associated with accessing human peritoneal effusion samples together with the technical challenges involved in maintenance and manipulation of primary patient-derived MCAs, these clinically relevant metastatic units remain understudied. Currently, techniques are available for generation of three-dimensional (3D) clusters from immortalized cell lines *in vitro*, which have been used predominantly to address hypoxia-, anoikis-, and chemoresistance [13–19]. The basic biology of MCA dynamics and cellular characteristics that dictate a metastatically successful MCA phenotype has yet to be elucidated.

Cadherins are a superfamily of calcium-dependent transmembrane adhesion molecules which mediate cell-cell adhesion, and maintain monolayer integrity and normal tissue architecture throughout the organism. In most epithelial tissues E-cadherin (Ecad) is responsible for the maintenance of cell-cell junctions. Loss of Ecad expression together with the acquisition of N-cadherin (Ncad) expression, designated epithelial-to-mesenchymal transition, is often associated with tumor progression and stromal invasion [20–22]. Mesenchymal-to-epithelial transition may be observed after extravasation and metastatic colonization [22]. In the healthy ovary, however, the mesodermally derived normal ovarian surface epithelium junctions are maintained exclusively by Ncad, whereas Ecad conditional coexpression is thought to be a sign of metaplasia [5,20,23–25].

Well-differentiated ovarian tumors express abundant Ecad, whereas advanced-stage and metastatic lesions exhibit upregulated Ncad expression [5,24–26]. Recent data also suggest human fallopian tube secretory epithelium as a possible progenitor of high-grade serous ovarian malignancies [27]. Normal tubal epithelial cells exhibit continuous expression of Ecad together with Ncad, whereas Ncad is lost in impaired atrophic tubal regions [28,29]. It has been reported that acquisition of Ecad enables MCAs to avoid detachment-induced apoptosis and resist radiation and chemotherapy [30–33]. Conversely, loss of Ecad via transcriptional or proteolytic mechanisms, induced by lysophosphatidic acid- or epidermal growth factor-related signaling, leads to increased detachment of EOC cells from the tumor surface [34–37]. As the contribution of cadherin switching to regulation of MCA dynamics and peritoneal invasion has not been examined, the objective of the current study is to comprehensively characterize the contribution of cadherin profiles to the behavior of free-floating EOC single cells and MCAs.

## Materials and Methods

### Cell Lines

The epithelial ovarian carcinoma cell lines OvCa433, OvCa429, OvCa432, and DOV13 were provided by Dr. Robert Bast (M.D. Anderson Cancer Center, Houston, TX) and maintained in minimal essential medium (Gibco) containing 10% fetal bovine serum (FBS; Gibco), 1% nonessential amino acids (Corning Cellgro), 1% penicillin/streptomycin (Lonza), 1% sodium pyruvate (Corning Cellgro), and 0.1% amphotericin B (Cellgro); DOV13 medium was additionally supplemented with 10 µg/ml of insulin (Gibco). The ovarian adenocarcinoma OVCAR3 and SKOV3 cell lines were purchased from American Type Culture Collection (Manassas, VA). OVCAR3 cell line was maintained in RPMI 1640 medium (Gibco) supplemented with 20% FBS, 1% sodium pyruvate, 1% nonessential amino acids, 1% GlutaMAX (Gibco), 1% penicillin/streptomycin, and 0.1% amphotericin B. SKOV3 cells were maintained in McCoy's 5a medium (Gibco) containing 10% FBS, 1% penicillin/streptomycin, 1% GlutaMAX, and 0.1% amphotericin B. Human mesothelial LP9 cell line was obtained from Coriell NIA Aging Cell Repository (Camden, NJ) and maintained in a 1:1 ratio of M199 and Ham F12 media (Gibco), supplemented with 15% FBS, 1% penicillin/streptomycin, 1% HEPES (Gibco), 1% GlutaMAX, 10 ng/ml of epidermal growth factor (Sigma), and 400 ng/ml of hydrocortisone. Cell lines were tested and authenticated by Genetica DNA Laboratories using short tandem repeat DNA profiling and were found to be >95% concordant. Red fluorescent protein (RFP) lentiviral vector (GenTarget, San Diego, CA) and green fluorescent protein (GFP) lentiviral vector (AddGene, Cambridge, MA) were utilized to create tagged OvCa433-RFP and SKOV3-GFP stable cell lines, respectively. Lentiviral transductions were performed according to manufacturers' protocols, and successfully labeled cells were further selected via BD FACSAria III cell sorter.

### Construction of a pmCherry:Ncad Plasmid

pmCherry-N1 vector was obtained from Clontech Laboratories, Inc. (Mountain View, CA). The murine Ncad-enhanced GFP construct was a gift from Dr. Cecile Gauthier-Rouviea. Ncad cDNA was subcloned into the pmCherry-N1 ApaI/AgeI sites using enzymes purchased from NEB, Inc. (Ipswich, MA). Gel purification of both the vector and insert was accomplished using the QiaQuick Gel

Extraction kit from Qiagen, Inc. (Redwood City, CA). Ligation was accomplished using T4 DNA Ligase (Promega Life Sciences, Madison, WI), and XL1-Blue supercompetent cells were transformed using the manufacturer's protocol (Stratagene, La Jolla, CA). Clones that yielded the correct size fragments with the double digest were sequenced to verify frame and sequence integrity using the following sequencing primers: pmCherry, forward: 5'-ggtaggcgtgtacggtggg-3'; pmCherry, reverse: 5'-ctgggtgcctcgtaggggcg-3'; and Ncad, forward: 5'-cagtagcggtaggggaccagg-3'. High-quality DNA for transfection was obtained using the Qiagen Plasmid Midi Kit.

#### *Hybrid OvCa433Ecad+/Ncad+ Cell Line Generation*

OvCa433 cells (Ecad+) were transfected with the Ncad expression vector to generate the hybrid OvCa433Ecad+/Ncad+ cell line (hereafter referred to as OvCa433Ncad+) by inserting a pmCherry:Ncad plasmid via electroporation utilizing the Human Keratinocyte Nucleofector kit and Nucleofector II device (Amaxa). Successfully transfected cell populations were observed under Olympus DSU-IX81 spinning disk confocal microscope, selected with OvCa433 medium containing 600  $\mu$ l/ml of G418 (Geneticin; ThermoFisher Scientific), and further sorted with BD FACSAria III cell sorter every 4 to 5 passages. Freshly sorted cells were utilized for all experiments.

#### *Hybrid SKOV3Ncad+/Ecad+ Cell Line Generation*

Ecad-RFP plasmid was kindly provided by Dr. Kathleen Green (Northwestern University, Chicago, IL). SKOV3 cells (Ncad+) were transfected with the Ecad expression vector to generate the hybrid SKOV3Ncad+/Ecad+ cell line (hereafter referred to as SKOV3Ecad+) by inserting an Ecad-RFP plasmid via chemical transfection using Lipofectamine 2000 reagent (Invitrogen) according to manufacturer's protocol specifications. Successfully transfected cell populations were observed under AMG EVOS fluorescence microscope, selected with SKOV3 medium containing 600  $\mu$ l/ml of G418 (Geneticin; ThermoFisher Scientific), and further sorted with BD FACSAria III cell sorter every 4 to 5 passages. Freshly sorted cells were utilized for all experiments.

#### *MCA Formation via Hanging Drop Method*

A hanging drop method was employed to generate 3D MCAs under cell free-floating condition in the absence of underlying adhesive substrate [18,38]. Briefly, EOC cells were cultured in 100-mm dishes to 90% to 95% confluence, washed once with phosphate-buffered saline (PBS; Cellgro) pH 7.4, and incubated with 1 ml of 0.25% Trypsin-EDTA (Corning Cellgro) for 3 to 4 minutes. Detached cells were harvested, centrifuged, and resuspended in fresh medium at 100,000 cells/ml. Droplets (20  $\mu$ l) were seeded on inner surface of a 150  $\times$  25-mm tissue culture dish lid (2000 cells per droplet). PBS was added to the lower dish, and the lid was gently inverted and placed on top of the dish. Cells were incubated at 37°C for 48 hours, and MCA formation was confirmed under the light microscope.

#### *Quantitative Polymerase Chain Reaction of cDNA Arrays*

Ovarian cancer TissueScan cDNA arrays (HORT-01) were obtained from OriGene. cDNA (5  $\mu$ l) in iTaq Universal SYBR Green Supermix (20  $\mu$ l, Bio-Rad) and gene-specific primers (200 nM) were run on a Bio-Rad Thermal iCycler device using a five-cycle protocol. The primer oligonucleotide pairs were obtained from Integrated DNA Technologies, Inc.: Ecad, forward: 5'-gccaagcagcagctacattctacagc-3' and reverse:

5'-gctgttcttcacgtctcaaatcc-3'; Ncad, forward: 5'-gtgccattagccaagggaattcagc-3' and reverse: 5'-gcgttctgttccactcataggagg-3'; and house-keeping glyceraldehyde 3-phosphate dehydrogenase (GAPDH), forward: 5'-acgaccattgtcaagctc-3' and reverse: 5'-ggctacatggcaactgga-3' [39].

#### *Western Blot Analysis*

Cells were grown to 95% to 100% confluence, washed twice with PBS, and incubated with ice-cold modified radioimmunoprecipitation assay lysis buffer (50 mmol/l Tris pH 7.5, 150 mmol/l NaCl, 0.1% SDS, 1% Triton X-100, 5 mmol/l EDTA)  $\times$  10 minutes at 4°C. Protein concentrations of the resulting lysates were calculated using the Bio-Rad DC protein assay kit. Lysates (20  $\mu$ g) were electrophoresed on an 9% SDS-polyacrylamide gel, transferred to a polyvinylidene difluoride membrane (Immobilon-P, Millipore) using a BioRad Trans-Blot SD Semi-Dry Transfer Cell device, and blocked in 3% bovine serum albumin (BSA) in TBST buffer (25 mmol/l Tris pH 7.5, 150 mmol/l NaCl, 0.1% Tween 20) for 1 hour at room temperature (RT). Blots were incubated overnight with mouse monoclonal anti-Ncad (#33-3900, Invitrogen), rabbit monoclonal anti-Ecad (#ab40772, Abcam), or mouse monoclonal anti-RFP (#GTX628898, GeneTex) primary antibody, 1:1000 dilution, in 3% BSA/TBST overnight at 4°C; washed with TBST 3  $\times$  5 minutes; and further incubated with the peroxidase-conjugated goat anti-mouse (#A4416, Sigma-Aldrich) or goat anti-rabbit (#A6667, Sigma-Aldrich) immunoglobulin G secondary antibody, 1:4000 dilution, in 3% BSA/TBST for 30 minutes at RT. The antibody-tagged protein bands were developed with SuperSignal West Dura chemiluminescent extended duration substrate kit (ThermoScientific) and visualized with the ImageQuant LAS4000 biomolecular imager. For GAPDH housekeeping gene loading control confirmation, membranes were incubated in a 400-mmol/l glycine pH 2.5 stripping buffer for 30 minutes; blocked again in 3% BSA/TBST; and reprobbed with the peroxidase-conjugated mouse monoclonal anti-GAPDH antibody (#G9295, Sigma-Aldrich), 1:25,000 dilution, in 3% BSA/TBST overnight at 4°C.

#### *Dual-Label Immunofluorescence Microscopy (DLIF)*

For DLIF of cell monolayers, OvCa433, OvCa429, DOV13, SKOV3, OvCa432, and OVCAR3 cells were subcultured on poly-L-lysine (Sigma-Aldrich) precoated cover slips, fixed with 10% formalin in PBS  $\times$  10 minutes, washed with PBS, and permeabilized with 0.3% Triton X-100 in PBS  $\times$  5 minutes at RT. For DLIF of ovarian cancer tissue microarrays (TMAs), OV809 array slides (US Biomax, Inc.) were deparaffinized with xylene 2  $\times$  10 minutes, hydrated with a decreasing series of ethanol concentrations (100% for 2  $\times$  2 minutes, 90% for 1 minute, 80% for 1 minute, 80% for 1 minute, 70% for 1 minute), rinsed with distilled water, and placed in PBS; antigen retrieval was performed with 10 mM sodium citrate pH 6.0 for 1 minute in a microwave, followed by 30-minute cooldown at RT. Subsequently, both cell monolayers and TMA sections were rinsed with 0.05% Tween 20 in PBS 2  $\times$  2 minutes; blocked with 5% normal goat serum (Sigma-Aldrich) for 1 hour at RT; and incubated in a 1:1 ratio mixture of two primary antibodies (for TMA: rabbit anti-Ecad #ab40772, Abcam; for cultured cells: rabbit anti-Ecad #07-697, Upstate; mouse anti-Ncad #33-3900, Invitrogen), 1:300 dilution, in 5% normal goat serum, 75 to 100  $\mu$ l per sample for 1 hour at RT or at 4°C overnight. After 3  $\times$  5-minute washes with 0.05% Tween 20 in PBS, samples were incubated in a 1:1 ratio mixture of two fluorescent-conjugated secondary antibodies (goat

anti-rabbit Alexa Fluor 488, Invitrogen; goat anti-mouse Alexa Fluor 594, Invitrogen), 1:500 dilution in PBS, 75 to 100  $\mu$ l per sample for 30 minutes at RT, and washed again with 0.05% Tween 20 in PBS for 3  $\times$  5 minutes. DAPI counterstaining and mounting were performed with Vectashield (Vector Laboratories, Inc.) for 20 minutes. Imaging was conducted using an Olympus DSU-IX81 spinning disc confocal microscope or a Leica DM5500 fluorescence microscope. Immunofluorescence microscopy of parental OvCa433 and SKOV3 cell lines and their transfected subclones, OvCa433N-cad+ and SKOV3Ecad+, grown on cover slips, was performed similarly by labeling with primary antibody (rabbit anti-Ecad #ab40772, Abcam, or mouse anti-Ncad #33-3900, Invitrogen), 1:300 dilution at 4°C overnight, and secondary antibody (goat anti-rabbit Alexa Fluor 488, Invitrogen, or goat anti-mouse Alexa Fluor 488, Invitrogen, respectively), 1:500 dilution, 30 minutes at RT, followed by DAPI counterstaining and imaging with Leica DM5500 fluorescence microscope. In some cell line experiments, exogenously expressed Ecad was also visualized using the RFP tag, with resulting images visualized in green for consistency.

### *MCA and Tissue Scanning Electron Microscopy (SEM)*

MCAs were generated via the hanging drop method as described, collected into 50-ml Falcon tubes by washing the drops gently from the dish lid surface with PBS three times, and centrifuged at 4000 rpm  $\times$  15 minutes at 22°C. MCA pellets were resuspended in a primary fixative solution (2% glutaraldehyde, 2% paraformaldehyde in 0.1 M cacodylate buffer pH 7.35) and rotated for 1 hour at RT in Eppendorf tubes. Samples were further washed with 0.1 M cacodylate buffer  $\times$  5 minutes and centrifuged; MCA pellets were evenly distributed in 100  $\mu$ l of cacodylate buffer, placed on top of poly-L-lysine-coated cover slips, and incubated for 30 minutes at RT. Primary fixation of mouse peritoneal explants was performed in primary fixative solution overnight at 4°C, followed with 3  $\times$  20-minute washes in 0.1 cacodylate buffer. Secondary processing of both MCA and tissue samples was done with 2% osmium tetroxide in 0.1 cacodylate buffer using a PELCO EM Pro Microwave vacuum chamber. Samples were then washed with ultrapure water 3  $\times$  5 minutes; dehydrated in a series of increasing ethanol concentrations (20%, 50%, 70%, 90%, 3  $\times$  100%), followed by critical point drying using Autosampdri-815A or Tousimis-931 dryer; placed on carbon stubs; and sputter coated with platinum or iridium. Samples were examined under FEI-Magellan 400 or Hitachi S-4700 field emission scanning electron microscopes.

### *Transmission Electron Microscopy (TEM)*

OvCa433 and DOV13 MCAs were generated, collected, and fixed with primary fixative. Sample pellets were further washed with 0.1 M cacodylate buffer  $\times$  5 minutes and encapsulated in prewarmed HistoGel at 4°C. After complete hardening, samples were washed once with cacodylate buffer, rinsed with 0.01 M mercaptoethanol and 0.13 sucrose in 0.1 M cacodylate buffer pH 7.35 (ME buffer) 20 minutes  $\times$  3 times on rocker, and then fixed with 1% osmium tetroxide using a PELCO EM Pro Microwave vacuum chamber. After three quick rinses with ME buffer, 3  $\times$  5-minute washes with ultrapure water, samples were dehydrated in a series of increasing concentrations of ethanol, followed by dehydrating in 100% acetone  $\times$  3 times, Epon/Spurr's resin infiltration, mold embedding, and polymerization at 60°C for 24 hours. Ultrathin sections were cut using a Reichert Ultracut microtome, mounted on 100-mesh nickel

grids, stained with 5% uranyl acetate and lead Sato's triple lead stain, and examined under JEOL 1400 transmission electron microscope.

### *Staining of Cells with Transient Fluorescent Dye*

Green 5-chloromethylfluorescein diacetate (CMFDA; Invitrogen) and red 4-({[4-(chloromethyl)phenyl]carbonyl}amino)-2-(1,2,2,4,8,10,10,11-octamethyl-10,11-dihydro-2H-pyrano [3,2-g:5,6-g']diquinoln-1-ium-6-yl)benzoate CellTrackers (CMTPX; Invitrogen) were utilized for short-term fluorescent labeling of cells. Briefly, cells were grown to 60% to 70% confluence, washed with serum-free medium (SFM), and incubated in 3 to 4 ml of fresh SFM supplemented with 1:1000 of corresponding CellTracker dye for 1 hour with subsequent change to fresh full medium for another 1 hour. Successful green or red staining was observed under AMG EVOS fluorescent microscope or Olympus DSU-IX81 spinning disc confocal microscope.

### *Mixed MCA Generation*

OvCa433, OvCa429, DOV13, SKOV3, and OvCa433Ncad+ cell lines were transiently stained with fluorescent CellTrackers. Red:green cell mixtures were then generated using the following proportions: 100%:0%, 75%:25%, 50%:50%, 25%:75%, and 0%:100%. Mixed cells were then seeded in 20- $\mu$ l hanging drops, and MCAs were observed at 48 hours using an AMG EVOS fluorescent microscope or Olympus DSU-IX81 spinning disc confocal microscope.

### *Cell Proliferation Assay*

Cells were seeded at 200,000 cells/dish in 35-mm dishes, incubated for 48 or 96 hours, washed twice with PBSS, trypsinized, harvested, and enumerated using a hemocytometer. The assay was repeated in triplicate, and statistical analysis was performed using a Student's *t* test.

### *Cell Migration Assay*

Cells were preincubated in SFM for 3 hours or overnight, diluted in fresh SFM at 500,000 cells/ml, and 500- $\mu$ l volume was applied on 24-well Boyden chamber membranes (6.5 mm, pore diameter 8.0  $\mu$ m; Costar). The inserts were placed in 24-well dishes filled with 750  $\mu$ l of SFM in each well and incubated for 5 and 12 hours. Cells were then fixed and stained on membranes using Diff-Quik kit (Siemens), and the number of migrated cells was enumerated. To account for differences that may be caused by unequal adhesiveness between wild-type and transfected cells, a 24-hour adherent cells control was performed by seeding 500  $\mu$ l of cells (500,000-cells/ml concentration) in rat tail collagen type I (RTCI; Corning)-precoated 24-well dishes, followed by 24-hour incubation, Diff-Quik kit fixation/staining, and enumeration of total cells adhered. The assay was repeated in triplicate, and statistical analysis was conducted using a Student's *t* test.

### *Matrigel Invasion Assay*

Cells were preincubated in SFM for 3 hours or overnight, diluted in fresh SFM at 500,000 cells/ml, and 500- $\mu$ l volume was applied on 24-well Boyden chamber membranes (6.5 mm, pore diameter 8.0  $\mu$ m; Costar) covered with preconstructed 3D Matrigel layer (1 mg/ml, 100  $\mu$ l/insert  $\times$  1-hour incubation at RT; BD Biosciences). The inserts were placed in 24-well dishes filled with 750  $\mu$ l of SFM and incubated for 36 and 72 hours. Cells were then fixed and stained on membranes using Diff-Quik kit (Siemens) and enumerated. The 24-hour adherent cell control was conducted as described above for

the cell migration assay. The assay was repeated in triplicate, and statistical analysis was performed using a Student's *t* test.

#### Cell-to-Collagen Adhesion Assay

Cells were diluted to 100,000 cells/ml and 500  $\mu$ l seeded on top of RTCI-precoated (10  $\mu$ g/ml in 0.1 M sodium carbonate pH 9.6; Corning) 24-well dishes and incubated for 10 to 60 minutes, then fixed and stained with Diff-Quick Kit (Siemens) and adherent cells enumerated. The assay was repeated in triplicate, and statistical analysis was performed using a Student's *t* test.

#### Cell-to-Mesothelium Adhesion Assay

An organotypic mesomimetic model was utilized to monitor cell-to-mesothelium adhesion [40]. OvCa433Ncad+ and SKOV3Ecad+ cells were transiently stained with red CMTPX or green CMFDA (Invitrogen), respectively. Parental OvCa433 and SKOV3 cells were RFP- or GFP-tagged, respectively, as described. Cells were applied to LP9 human mesothelial monolayers in RTCI-precoated (Corning) 24-well dishes at 200,000 cells/ml (1ml total), incubated for 30 or 60 minutes, washed 3 $\times$  with PBS washes, and imaged with AMG EVOS fluorescence microscope. Image analysis was performed using *ImageJ*. The assay was repeated in triplicate, and statistical analysis was performed using a Student's *t* test.

#### Cell-to-Peritoneum Adhesion Assay

Cell-to-peritoneum adhesion was assessed *ex vivo* as published previously [40,41]. Briefly, C56BL6 mice (Jackson Laboratories) were euthanized by CO<sub>2</sub> inhalation and subsequent cervical dislocation, then dissected using a ventral midline incision; four peritoneal tissue pieces were removed and pinned to the bottom of 24-well dishes precoated with optically transparent silicone using Sylgard 184 Silicone Elastomer Kit (Fisher). OvCa433Ncad+ and SKOV3Ecad+ cells were transiently stained with red CMTPX or green CMFDA (Invitrogen), respectively. Parental OvCa433 and SKOV3 cells were RFP- or GFP-labeled, respectively. Cells were applied to murine peritoneal explants, incubated for 1 to 2 hours, and washed with 3  $\times$  3-minute ice-cold PBS washes, and cells/peritoneum were imaged with AMG EVOS fluorescence microscope. Image analysis was performed with *ImageJ*. The assay was repeated in triplicate, and statistical analysis was performed using a Student's *t* test. The fourth replicate tissue explants were subjected to SEM processing and imaging as described above.

## Results

### Heterogeneous Cadherin Expression in Human EOC Tumors and Cell Lines

Human EOCs exhibit heterogeneous cadherin profiles, displaying both Ecad and Ncad immunoreactivity. We previously demonstrated Ecad staining in 86% of a cohort of primary human EOCs, whereas 33% were positive for Ncad and 28% were positive for both cadherins as assessed using serial sections [5]. Similar results were obtained by analysis of cDNA prepared from RNA isolated from human ovarian tumors (Figure 1 A). Of 41 ovarian cancer tissue samples, 95% (*n*=39) and 56% (*n*=23) were positive for expression of Ecad and Ncad, respectively. In this cohort, all Ncad-positive samples also expressed Ecad (56%). In a large cohort of tissues from ovarian carcinoma patients (*n*=70) assessed using DLIF, two unique patterns of cadherin staining are observed: "mixed cadherin," in which distinct cells within the same tumor express Ecad or Ncad, and "hybrid cadherin,"

wherein the same tumor cell(s) simultaneously expresses both cadherins (Figure 1 B). The human tumor data are recapitulated in a panel of human EOC cell lines as shown by DLIF (Figure 1 C) and Western blot analysis (not shown [5]), providing a relevant set of epithelial (Ecad+; OvCa433 and OvCa429), mesenchymal (Ncad+; DOV13 and SKOV3), and hybrid (Ecad+/Ncad+; OVCAR3 and OvCa432) cadherin cell phenotypes for mechanistic evaluation.

### Ultrastructural Analysis of MCAs

It has been demonstrated previously that free-floating MCAs differ in size, shape, and cohesivity from patient to patient [9,10,42]. Immunohistochemical analysis of EOC cells from human malignant effusions has also shown variability in cadherin expression, defining cells that are Ecad+, Ncad+, or hybrid cadherin; however, the correlation between cadherin composition and MCA morphology has not been interrogated [43]. To evaluate the contribution of cadherin profile to MCA phenotype, MCAs were generated *in vitro* via the hanging drop method [40] (Supplemental Figure 1A) using the panel of cell lines described above and were visualized using SEM (Figure 2) and TEM (Figure 3). Striking cadherin-dependent differences in aggregate surface morphology and interior ultrastructure were observed. Scanning electron micrographs show that whereas cells expressing mesenchymal-type cadherin (Ncad+ DOV13 and SKOV3) formed solid, smooth, cohesive spheroids, cells expressing epithelial-type cadherin (Ecad+ OvCa433 and OvCa429) formed loosely clustered aggregates covered by uniform microvilli. An intermediate surface phenotype was displayed by the hybrid cadherin (Ecad+/Ncad+ OvCa432 and OVCAR3) cell lines (Figure 2). Evaluation of MCA cross sections using TEM to examine aggregate interior ultrastructure revealed tightly compacted adherent aggregates in Ncad-expressing DOV13 cells, whereas Ecad+ OvCa433 clusters exhibited few cell:cell contacts, resulting in acellular regions in the aggregate cross section (Figure 3).

### Cadherin-Dependent Sorting and Mixing in Heterogeneous MCAs

Heterogeneous primary tumors will shed a population of cells with a variety of cadherin expression profiles; however, the ability of cells with distinct cadherin expression profiles to form MCAs has not been evaluated in EOC. As subsequent adhesion and colonization of mixed MCAs may represent a mechanism for generation of metastatic lesions with "mixed" cadherin profiles, experiments were performed to examine aggregates formed by mixing two distinct cell types. Cells were transiently stained with red or green fluorescent dyes and seeded together at varying ratios in hanging drops to generate mixed clusters (Supplemental Figure 1B). Aggregates formed by cells with distinct cadherin profiles, such as the mesenchymal-type DOV13 (Ncad+) and epithelial-type OvCa433 (Ecad+), demonstrated the propensity to sort into distinct MCAs based on cadherin expression profile, rather than forming heterogeneous clusters (Figure 4 A). In contrast, cell lines with common cadherin profiles [OvCa433/OvCa429 (Ecad/Ecad); DOV13/SKOV3 (Ncad/Ncad)] readily mixed to form homogeneous aggregates (Figure 4 B and C). Moreover, the hybrid cadherin OvCa432 (Ecad+/Ncad+) EOC line exhibits the ability to cluster with both OvCa433 (Ecad+) and DOV13 (Ncad+) cells (Supplemental Figure 2A and B). Quantitative analysis of mixed MCA formation is provided in Table 1. Interestingly, the presence of greater than one cell type in suspension resulted in a larger number of smaller MCAs relative to homogeneous controls.

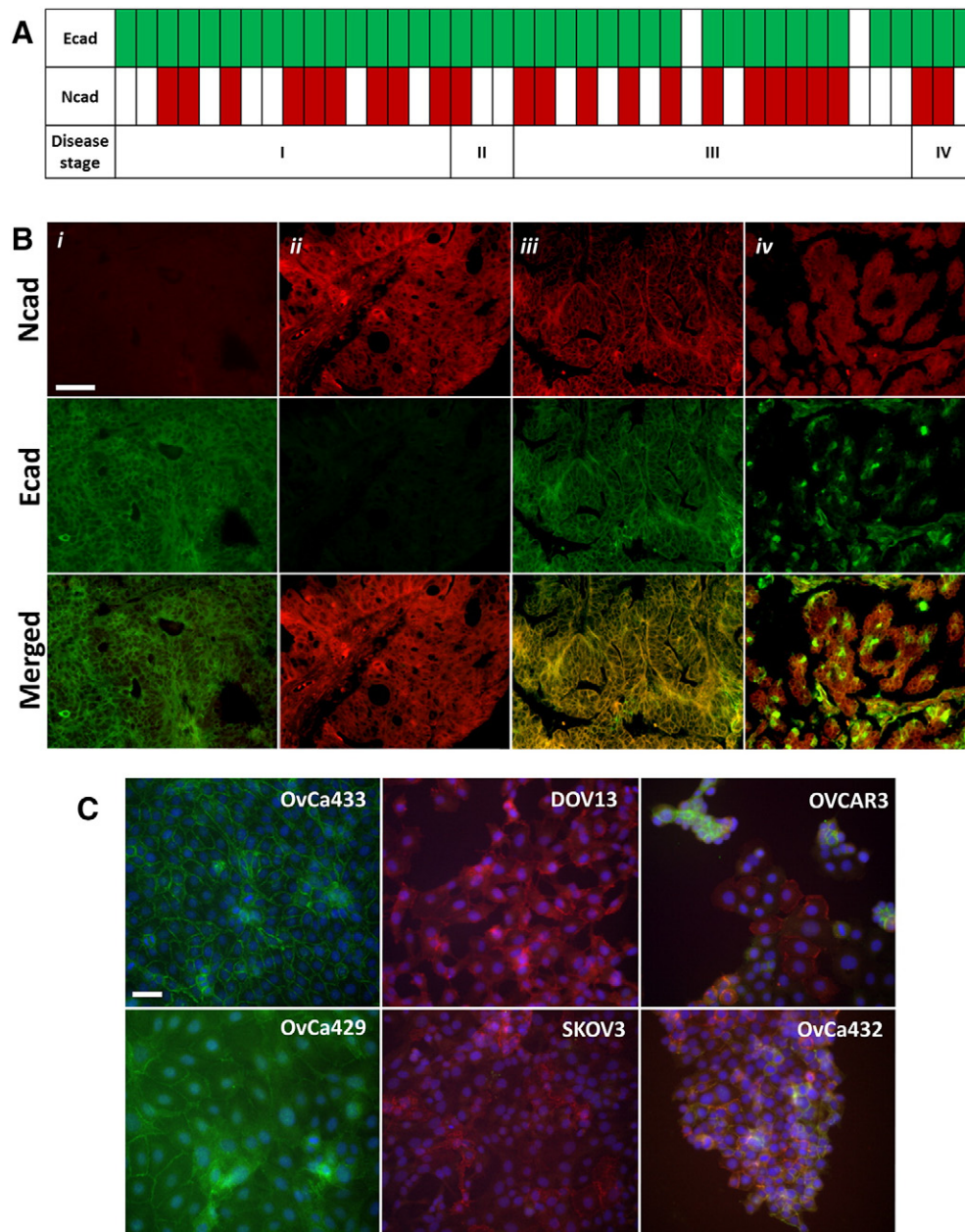


**Figure 1.** Human EOC tissues and cell lines demonstrate heterogeneous cadherin expression. (A) Ovarian cancer TissueScan cDNA arrays (HORT-01, OriGene) were analyzed on a Bio-Rad Thermal iCycler using an iTaq Universal SYBR Green Supermix (Bio-Rad) to test for Ecad and Ncad expression. Open rectangles show negative Ecad or Ncad expression (defined as no signal or  $C_t \geq 35$ ), and filled rectangles represent positive Ecad (green) or Ncad (red) expression (defined as  $C_t < 35$ ) in human ovarian carcinoma specimens, stages I, II, III, and IV (according to International Federation of Gynecology and Obstetrics) as indicated. (B) Microarrayed human TMA ovarian cancer tissues ( $n=70$  patients, OV809, US Biomax, Inc.) were double-stained for Ecad (green) and Ncad (red), as indicated in Methods. Representative images of ovarian serous papillary adenocarcinoma from the TMA showing examples of (i) predominant Ecad expression, (ii) predominant Ncad expression, (iii) hybrid cadherin expression (Ecad/Ncad within same cells), and (iv) mixed cadherin expression (Ecad/Ncad within different cells of the same tissue); scale bar:  $50 \mu\text{m}$ . Images were obtained using a Leica DM5500 microscope. (C) EOC cell lines OvCa433, OvCa429, DOV13, SKOV3, OVCAR3, and OvCa432 were subcultured on cover slips and processed for Ecad (green) and Ncad (red) dual-label immunofluorescence, nuclei-counterstained with DAPI (blue) as stated in Methods, and imaged using an Olympus DSU-IX81 microscope. Scale bar:  $50 \mu\text{m}$ .

#### Acquisition of the Hybrid Cadherin Phenotype and MCA Morphology

To model the acquisition of a “hybrid” cadherin phenotype observed during human EOC progression, in which an individual cell expresses both Ecad and Ncad, a hybrid cadherin cell line (OvCa433Ncad+) was generated on an epithelial cell background

(OvCa433) (Supplemental Figure 3, A, B, and E). Acquisition of Ncad expression resulted in the ability to form mixed heterotypic aggregates with Ncad+ DOV13 cells (Figure 5 A, Table 1). Examination of surface morphology of the hybrid cadherin MCA by SEM showed loss of uniform microvilli observed in the parental cell line together with increased cell surface lamellipodia and

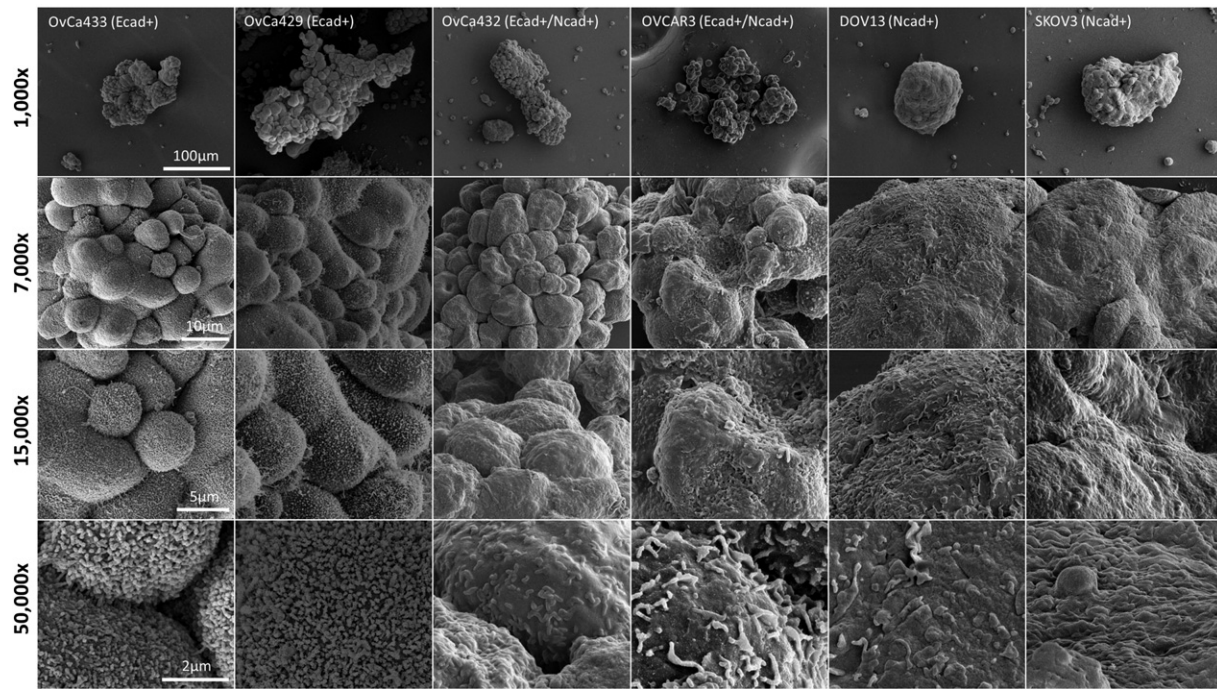


**Figure 2.** EOC cadherin profiles correlate with MCA surface morphology. MCAs were generated from OvCa433, OvCa429, OvCa432, OVCAR3, DOV13, and SKOV3 cells, as indicated, via the hanging drop method (Supplemental Figure 1A); processed for SEM as detailed in Methods; and examined using FEI-Magellan 400 or Hitachi S-4700 field emission SEM. Representative images were taken at 1000 $\times$ , 7000 $\times$ , 15,000 $\times$ , and 50,000 $\times$  magnifications (scale bars as indicated).

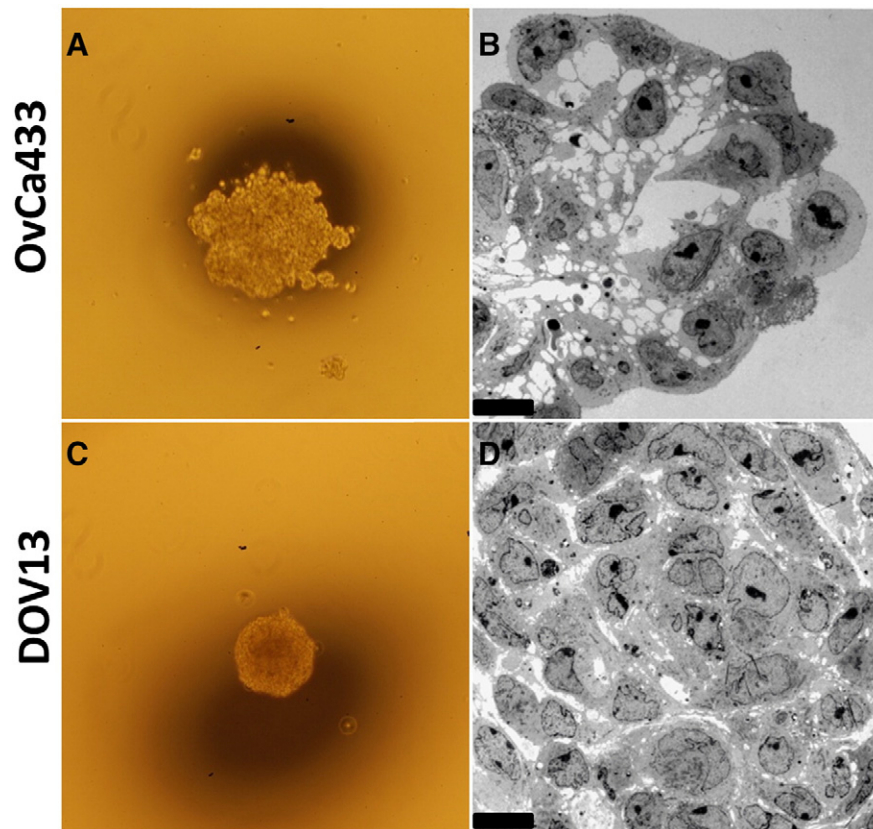


**Figure 3.** Epithelial- and mesenchymal-type MCAs differ in cross-sectional ultrastructure. Representative epithelial (A-B, OvCa433) and mesenchymal (C-D, DOV13) MCAs were generated via the hanging drop method (Supplemental Figure 1A), observed under light microscope at 4 $\times$  magnification (A and C), and further processed for TEM as detailed in Methods. Sections were examined under JEOL 1400 TEM (B and D). Scale bar: 10  $\mu$ m.

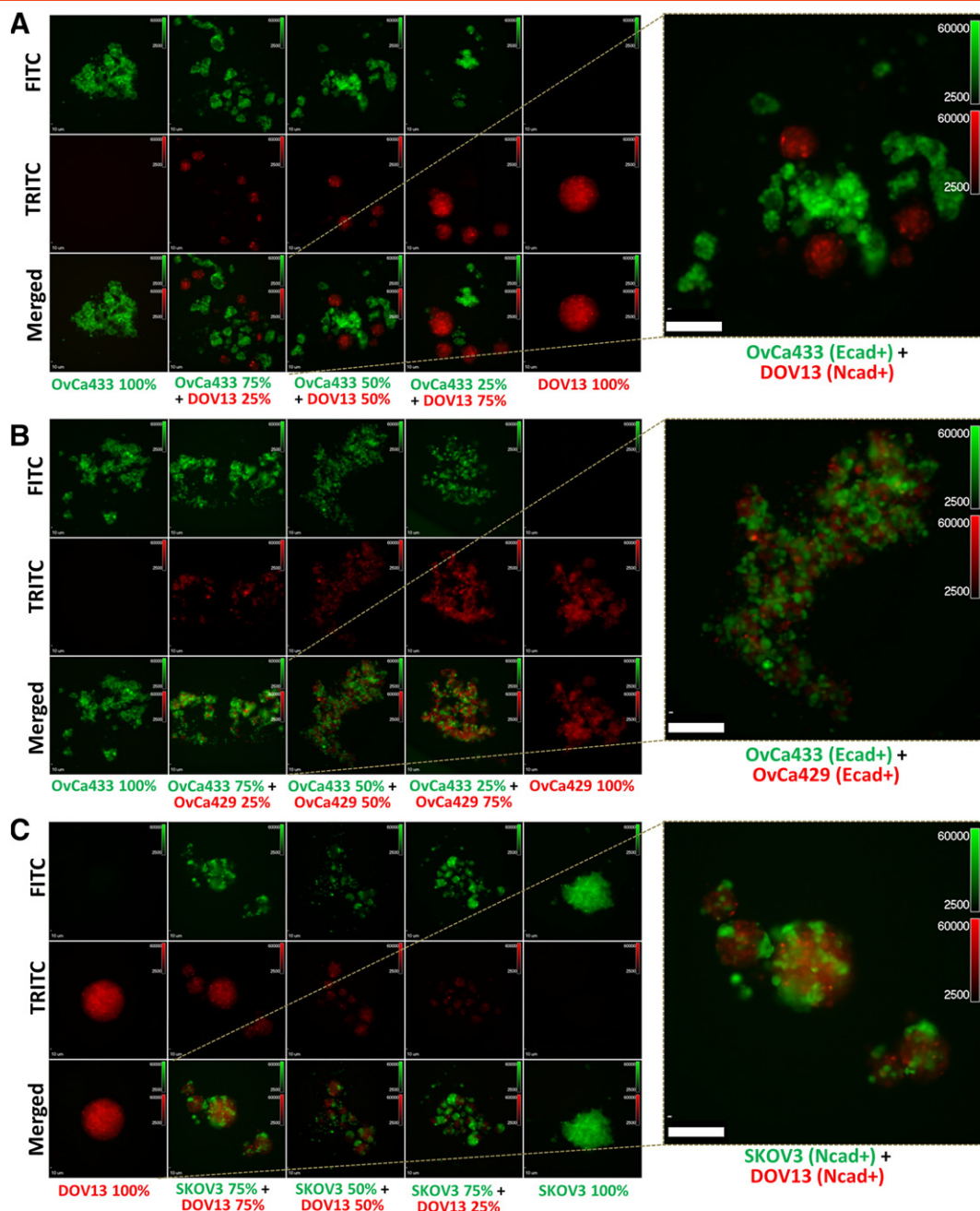


**Figure 4.** Cadherin profiles dictate cell sorting and mixing in heterogeneous MCAs. Cells were transiently fluorescently labeled with green or red dyes as described in Methods and cultured in hanging drops (100,000 cells/ml; Supplemental Figure 1B) at various proportions as indicated in the figure panels. (A) Green OvCa433 (Ecad+) mixed with red DOV13 (Ncad+); (B) green OvCa433 (Ecad+) mixed with red OvCa429 (Ecad+); (C) green SKOV3 (Ncad+) mixed with red DOV13 (Ncad+). MCAs were observed after 48 hours under Olympus DSU-IX81 spinning disc confocal microscope. Scale bar: 10  $\mu$ m. Right panels: A representative image is shown enlarged.

filopodia characteristic of a more migratory/invasive phenotype (Figure 5 B) [44,45].

#### *Acquisition of the Hybrid Cadherin Phenotype and MCA Behavior*

To examine the contribution of Ncad acquisition to cellular behavior, a panel of assays was used to compare metastasis-associated cellular activities using parental OvCa433 cells and the hybrid cadherin OvCa433Ncad+ line. Following shedding from the primary tumor, the intraperitoneal metastasis of EOC is characterized by initial adhesion of tumor cells and MCAs to the peritoneal mesothelial surface, wherein

they induce mesothelial cell retraction enabling metastatic cells to migrate and invade into the submesothelial collagen-rich matrix and proliferate to anchor secondary lesions (reviewed in [5,40]). Acquisition of Ncad expression resulted in an about 10-fold increase in adhesion to human peritoneal mesothelial cells grown in 3D organotypic mesomimetic cultures (Figure 6 A) [40]. Small but significant increases in motility were also observed together with a three-fold enhancement of invasive activity (Figure 6, B and C), although no significant difference in cell adhesion to collagen was noted (Supplemental Figure 4A). Additionally, OvCa433Ncad+ cells exhibited a proliferative advantage relative to OvCa433 parental controls (Figure 6 D).

**Table 1.** Quantitation of Mixed vs Sorted MCAs

| Cell Line 1     | Cell Line 2                | Mixed MCAs (%) | Sorted MCAs (%) |
|-----------------|----------------------------|----------------|-----------------|
| OvCa433 (Ecad+) | DOV13 (Ncad+)              | 0              | 100             |
| OvCa433 (Ecad+) | OvCa429 (Ecad+)            | 100            | 0               |
| DOV13 (Ncad+)   | SKOV3 (Ncad+)              | 95.8           | 4.2             |
| OvCa433 (Ecad+) | OvCa432 (Ecad+/Ncad+)      | 95.7           | 4.3             |
| DOV13 (Ncad+)   | OvCa432 (Ecad+/Ncad+)      | 90.2           | 9.8             |
| DOV13 (Ncad+)   | OvCa433Ncad+ (Ecad+/Ncad+) | 92.3           | 7.7             |

Cells were mixed at a 50:50 ratio of cell line 1 and cell line 2 and cultured in hanging drops as described in Methods. Aggregates forming in a minimum of 18 aggregates were evaluated per condition, and at least 3 replicates were performed. The percentage of total aggregates containing both cell types was defined as “% mixed MCAs,” whereas the percentage of aggregates containing a single cell type was defined as “% sorted MCAs.”

To further assess the effect of Ncad acquisition on early adhesive events in metastatic seeding, an *ex vivo* peritoneal tissue explant assay was utilized [40,41]. In this assay, live peritoneal explants are maintained *ex vivo* pinned to an optically clear Silastic resin and are incubated with fluorescently tagged tumor cells followed by fluorescence microscopy or SEM to quantify adherent cells (Figure 7 A). A

four- to five-fold increase in attachment of OvCa433Ncad+ cells to peritoneal tissue was observed relative to parental OvCa433 cells (Figure 7, B-D), supporting a role for Ncad expression in early metastatic dissemination.

To further examine the impact of the hybrid cadherin phenotype on cell behavior, an additional hybrid cadherin cell line (SKOV3Ecad+) was generated on a mesenchymal cell background (SKOV3) (Supplemental Figure 3, C, D, and F). Gain of Ecad expression altered MCA surface morphology as evidenced by loss of smooth spheroid-like appearance and gain of a more loosely aggregated phenotype analogous to the OvCa433Ncad+ hybrid cadherin MCAs (Figures 5 B and 8 A). Acquisition of Ecad also altered the adhesive phenotype, with hybrid cells exhibiting an about two-fold decrease in adhesion to collagen (Figure 8B), consistent with approximately two- to three-fold decreases in adhesion to human peritoneal mesothelial cells grown in 3D organotypic mesomimetic cultures (Figure 8 C), and to live murine peritoneal explants (Figure 8, D-F). No significant differences in migration and small changes in invasion were observed (Supplemental Figure 4, B and C). Moreover,

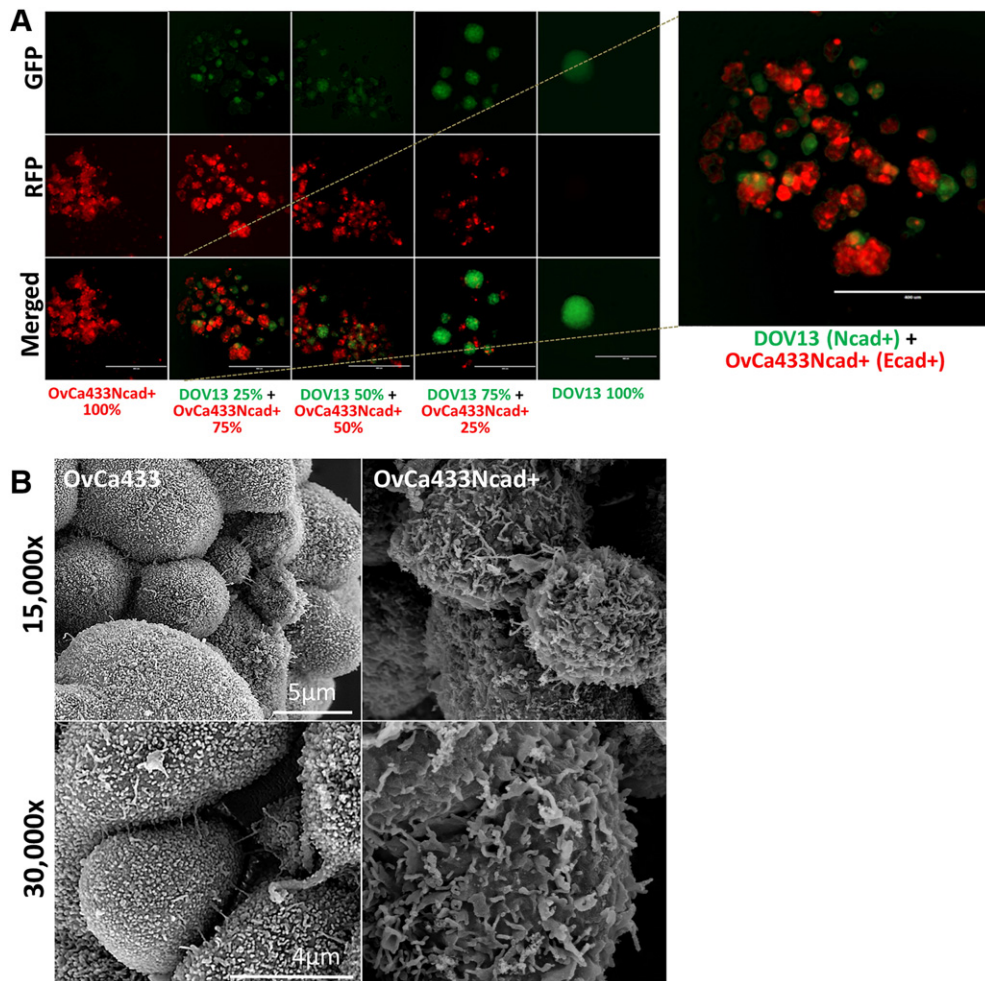


**Figure 5.** Acquisition of the hybrid cadherin phenotype induces mixed aggregate formation and alters MCA surface morphology. (A) Transiently stained hybrid cadherin cell line (OvCa433Ncad+, red) and DOV13 (Ncad+, green) cells were cocultured in hanging drops (100,000 cells/ml; Supplemental Figure 1B) at the proportions indicated in the figure panel. MCAs were observed at 48 hours under AMG EVOS fluorescence microscope. Scale bar: 400  $\mu$ m. Right panel: A representative image is shown enlarged. (B) OvCa433 and hybrid OvCa433Ncad+ MCAs were generated via the hanging drop method (Supplemental Figure 1A) and processed for SEM as described in Methods. Microscopy was performed using Hitachi S-4700 field emission SEM. Representative images were taken at 15,000 $\times$  and 30,000 $\times$  magnifications (scale bars as indicated).

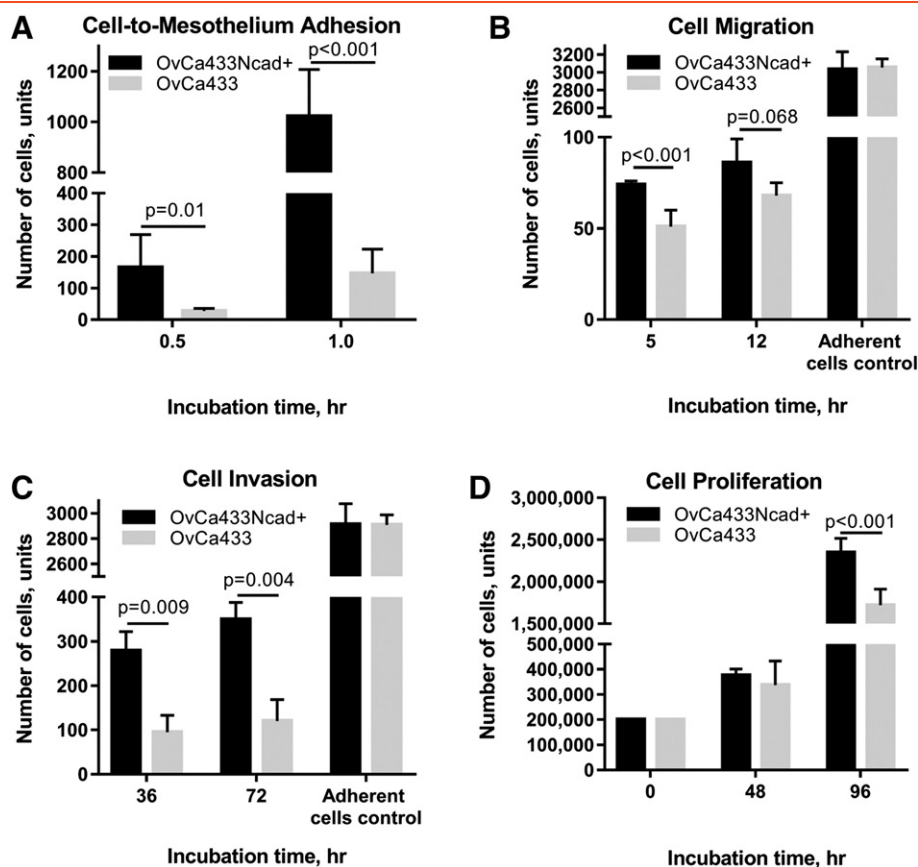


**Figure 6.** Acquisition of Ncad expression promotes adhesive, migratory, invasive, and proliferative cell properties. (A) Evaluation of tumor cell:mesothelial cell adhesion: Mesomimetic cultures comprised of LP9 human mesothelial cell monolayers cultured on type I collagen gels in 24-well plates were incubated with either OvCa433-RFP (grey bars) or transiently dyed hybrid OvCa433Ncad+ cells (200,000 cells/ml) (black bars) for 0.5 or 1 hour, as indicated. After washing, adherent cells were imaged with AMG EVOS fluorescence microscope at 4 $\times$  magnification  $\times$  6 fields of view; image analysis was performed using *ImageJ*. (B) Evaluation of tumor cell migration. OvCa433 (grey bars) and hybrid OvCa433Ncad+ cells (black bars) were preincubated in SFM for 3 hours prior to seeding onto Boyden chamber membranes (at 500,000 cells/ml, 500  $\mu$ l) for 5 or 12 hours as indicated. Cells migrating to the lower side of the filter were then fixed and stained with the Diff-Quik (Siemens) and enumerated under light microscope at 10 $\times$  magnification  $\times$  6 fields of view. An adherent cell control was conducted simultaneously, as described in Methods, to assess whether alterations in cell adhesion contributed to the differential migratory behavior observed. (C) Analysis of cellular invasion. OvCa433 (grey bars) and OvCa433Ncad+ cells (black bars) were incubated in SFM for 3 hours prior to seeding on top of 3D Matrigel constructs inside Boyden chambers (at 500,000 cells/ml, 500  $\mu$ l) for 36 or 72 hours as indicated. Cells invading to the lower side of the filter were then fixed and stained with Diff-Quik and enumerated under the light microscope at 10 $\times$  magnification  $\times$  6 fields of view. An adherent cell control was conducted simultaneously, as described in Methods, to assess whether alterations in cell adhesion contributed to the differential invasive behavior observed. (D) Analysis of cell proliferation. OvCa433 (grey bars) and OvCa433Ncad+ (black bars) cells were seeded in 35-mm dishes (200,000 cells/dish) and incubated for 48 or 96 hours as indicated prior to enumeration of cells using hemocytometry. All assays were repeated in triplicate, and statistical analysis was conducted using a Student's *t* test.

hybrid SKOV3Ecad+ cells demonstrated enhanced proliferation relative to SKOV3 parental controls (Figure 8 G).

## Discussion

Relative to most solid tumors, EOC demonstrates a unique metastasis mode via direct extension into the peritoneal cavity as well as exfoliation from the primary tumor and subsequent dissemination of single cells and MCAs in ascites fluid [6]. Originating either from Ncad+ ovarian surface epithelium which has undergone metaplastic mesenchymal to epithelial changes or from the fallopian tube epithelium, which initially expresses Ecad and Ncad, primary EOC tumors exhibit significant cadherin heterogeneity, ranging from purely Ecad+ or Ncad+ neoplasms to both "mixed cadherin" and "hybrid cadherin" phenotypes [5]. Released from the primary tumor

surface, ovarian cancer cells and/or cell sheets create a heterogeneous pool of free-floating metastatic units with diverse cadherin profiles which are readily detected in carcinomatous effusions [43]. Nevertheless, a limited fraction of ovarian cancer MCAs found in malignant ascites is reported to be invasive [12]. The current study was designed to model and comprehensively characterize the impact of cellular cadherin composition on free-floating cell/MCA behavior. Here, we report cadherin-dependent diversity in cell-cell interactions, MCA formation, aggregate surface morphology, and aggregate interior ultrastructure. Our results support a previous study of brain tumor cell lines with low, intermediate, or high levels of Ncad expression, which demonstrated formation of unstable poorly cohesive, intermediately cohesive, or compact smooth 3D spheroids, respectively [46]. Such dramatic phenotypic variation suggests that

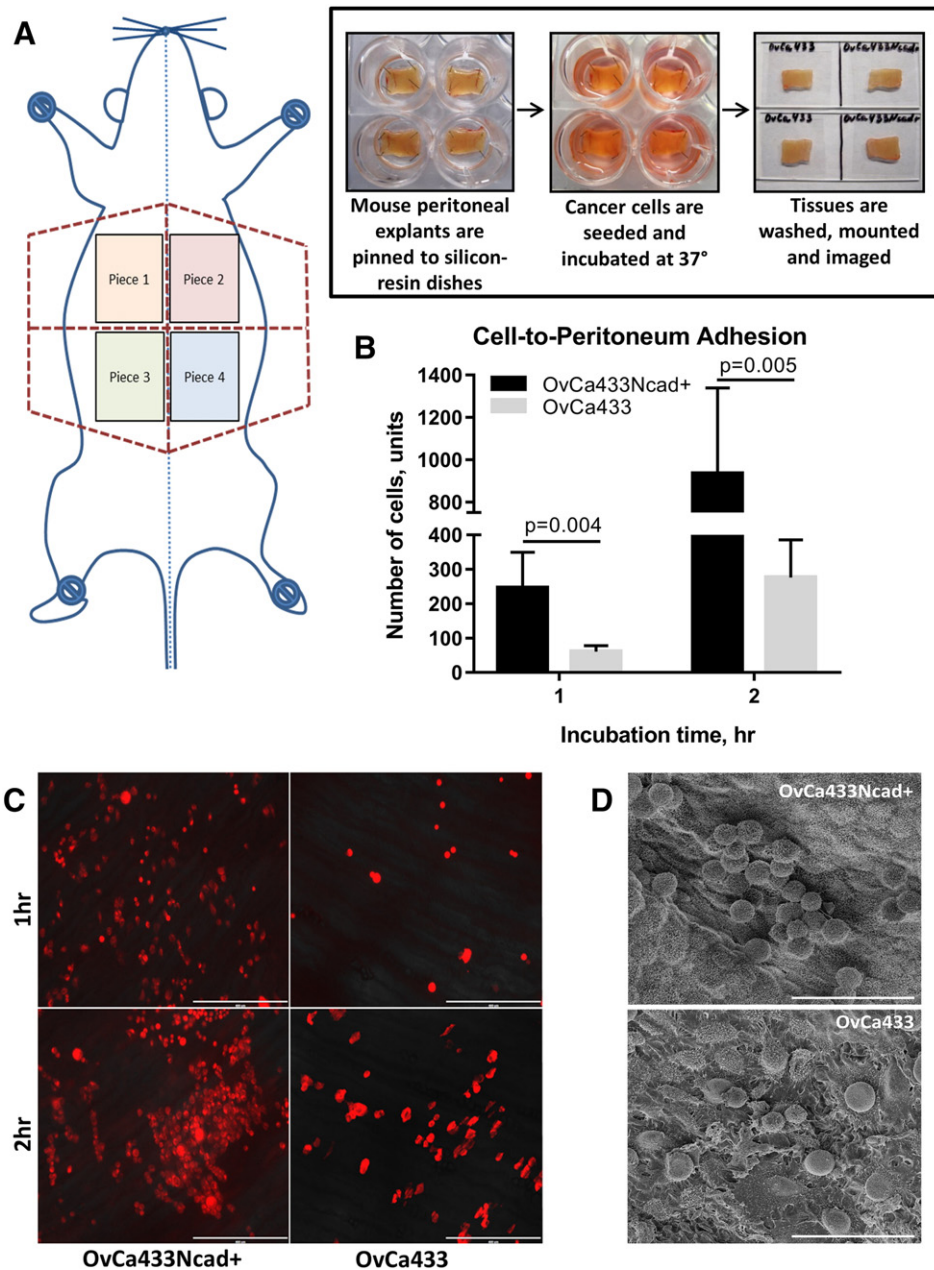


**Figure 7.** Acquisition of Ncad enhances adhesion to peritoneal explants. (A) Overview of *ex vivo* adhesion assay. Explants of peritoneal tissue were dissected and pinned "mesothelium-side-up" on optically clear Silastic resin as described in Methods for use as an adhesive substratum. Stably tagged OvCa433-RFP or transiently dyed OvCa433Ncad+ cells (as described in Methods) were incubated with peritoneal tissue explants for 1 or 2 hours as indicated, rinsed with ice-cold PBS 3 × 3 minutes, mounted inverted on glass slides, and imaged. (B-C) Adherent cells (OvCa433, grey bars; OvCa433Ncad+, black bars) were enumerated using an AMG EVOS fluorescence microscope at 4× magnification × 6 fields of view with image analysis conducted in *ImageJ*. The assay was repeated in triplicate, and statistical analysis was performed using a Student's *t* test. (D) Tissue explants from a separate replicate were subjected to SEM processing and imaged with FEI-Magellan 400 at 15,000× and 30,000× (scale bars as indicated).

alterations in cadherin profiles may influence the MCA response to hypoxic conditions and susceptibility to therapeutic drugs due to variability in their cohesivity and surface complexity.

It has been widely accepted for decades in the developmental biology literature that cocultured cells with different cadherin profiles will spontaneously segregate and reorganize, maintaining cadherin subtype-specific binding. This "differential adhesion hypothesis" explains the cell sorting phenomenon from the point of thermodynamic stability, wherein cells position themselves near cells with similar/equivalent adhesive strength in order to achieve maximum

cell-cell binding strength and minimize the interfacial free energy. This process of selective adhesion, first observed in embryonic amphibian cells [47,48], was later experimentally verified using a series of multicellular systems and cadherin-transfected cell lines [49]. More recently, computational models simulating adhesion-mediated morphogenesis were used to confirm this hypothesis [50,51], which is now widely believed to be applicable to malignant cells and tissues as well. Recently, however, contradictory data have emerged showing novel adherens junctions containing heterodimeric complexes of Ecad/Ncad in endoderm-derived normal and malignant tissues

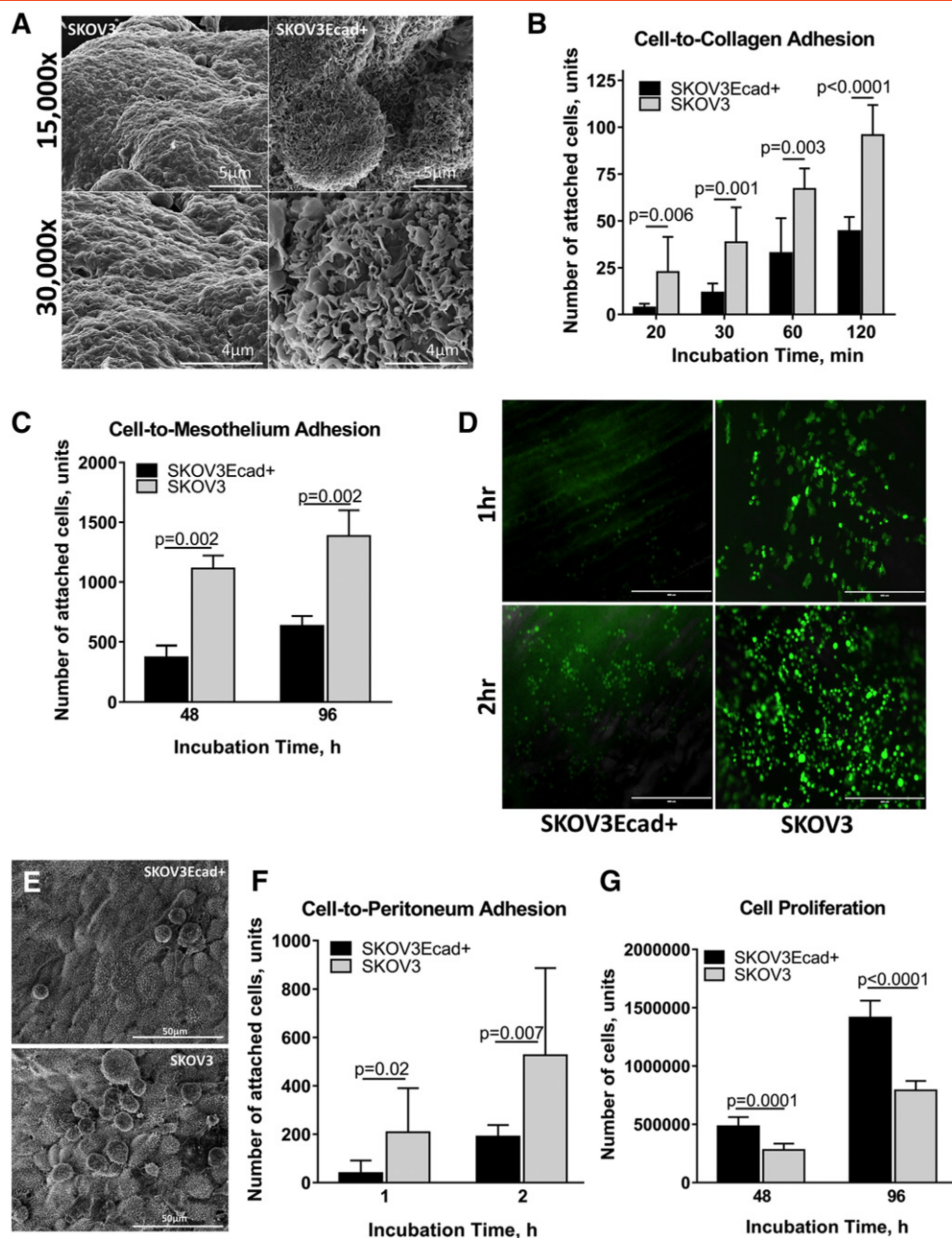


**Figure 8.** Acquisition of Ecad expression alters MCA morphology, attenuates cell adhesive behavior, and increases cell proliferation. (A) SKOV3 and hybrid SKOV3Ecad+ MCAs were generated via the hanging drop method (Supplemental Figure 1A) and processed for SEM as described in Methods. Microscopy was performed using FEI-Magellan 400 with representative images taken at 15,000 $\times$  and 30,000 $\times$  magnifications (scale bars as indicated). (B) Evaluation of cell-to-collagen adhesion. SKOV3 (grey bars) and SKOV3Ecad+ (black bars) cells were incubated on top of type I collagen–precoated (10  $\mu$ g/ml) 24-well dishes (at 100,000 cells/ml, 500  $\mu$ l) for 20, 30, 60, and 120 minutes, as indicated, followed by washing, fixation, staining with Diff-Quick (Siemens), and enumeration of adherent cells under light microscope at 10 $\times$  magnification  $\times$  6 fields of view. The assay was repeated in triplicate and statistical analysis performed using a student's *t*-test. (C) Evaluation of tumor cell:mesothelial cell adhesion: Meso-mimetic cultures comprised of LP9 human mesothelial cell monolayers cultured on type I collagen gels in 24-well plates were incubated with either SKOV3-GFP (grey bars) or transiently dyed hybrid SKOV3Ecad+ cells (200,000 cells/ml) (black bars) for 0.5 or 1h, as indicated. After washing, adherent cells were imaged with AMG EVOS fluorescence microscope at 4 $\times$  magnification  $\times$  6 fields of view; image analysis was performed using *ImageJ*. (D) Assessment of cell-to-peritoneum adhesion. Explants of peritoneal tissue were dissected and pinned “mesothelium-side-up” on optically clear Silastic resin as described in Methods for use as an adhesive substratum. Stably tagged SKOV3-GFP or transiently dyed SKOV3Ecad+ cells (as described in Methods) were incubated with peritoneal tissue explants for 1 or 2 hours as indicated, rinsed with ice-cold PBS 3  $\times$  3 minutes, mounted inverted on glass slides, and imaged with AMG EVOS fluorescence microscope. (E) Tissue explants from a separate replicate were subjected to SEM processing and imaged with FEI-Magellan 400 at 15,000 $\times$  and 30,000 $\times$  (scale bars as indicated). (F) Quantitative evaluation of cell-to-peritoneum adhesion (SKOV3, grey bars; SKOV3Ecad+, black bars) was performed using an AMG EVOS fluorescence microscope at 4 $\times$  magnification  $\times$  6 fields of view with image analysis conducted in *ImageJ*. The assay was repeated in triplicate, and statistical analysis was performed using a Student's *t* test. (G) Analysis of cell proliferation. SKOV3 (grey bars) and SKOV3Ecad+ (black bars) cells were seeded in 35-mm dishes (200,000 cells/dish) and incubated for 48 or 96 hours as indicated prior to enumeration of cells using hemocytometry. All assays were repeated in triplicate, and statistical analysis was conducted using a Student's *t* test.

including liver parenchyma, bile and pancreatic duct cells, and gall bladder epithelium [52]. Similar results have been obtained using various tumor-derived cell cultures [52]. In one interesting recent study, the noninvasive normal breast epithelial cell line MCF-10A (Ecad+) was cocultured with the malignant breast cell line MDA-MB-231 (Ecad-), successfully forming a heterotypic aggregate from which the noninvasive MCF-10A cells followed the invasive MDA-MB-231 “cell leaders” through collagen gels [53].

Our data revealing heterogeneous cadherin expression patterns in primary EOC tumors and ascites (current study and [5]) raised the question of whether differential cadherin expression would preclude or promote clustering into heterotypic MCAs that subsequently adhere to seed secondary lesions. The current data demonstrate selective cadherin-dependent sorting of cells expressing mesenchymal-type cadherins (Ncad+) from those with epithelial-type cadherins (Ecad+), suggesting that the cadherin heterogeneity observed in peritoneal lesions may occur as a result of seeding of distinct MCAs in the metastatic niche. Alternatively, soluble or cellular factors prevalent in the peritoneal microenvironment may induce switching of cadherin expression in the secondary lesions. Interestingly, however, cells with the “hybrid cadherin” phenotype, in which both Ecad and Ncad are expressed in the same cell, are able to form mixed MCAs with both epithelial and mesenchymal cells and thus may play key role in recruiting a heterogeneous cell population to the metastatic site. Moreover, the dual cadherin phenotype may also be advantageous over a purely epithelial or mesenchymal one due to its plastic, “metastable,” less differentiated state [54]. It has been suggested that the plasticity of such hybrid (partial epithelial-to-mesenchymal transition or semi-mesenchymal) cells allows them to modulate their differentiation state depending on the environmental cues [54–57]; gain *de novo* and adaptive drug and radiation resistance [54,58–60]; and proliferate, creating a pool of new hybrid cells as well as completely differentiated cells [61]. Our data indicate that both expression of Ecad in the mesenchymal-type cells and acquisition of Ncad by the epithelial-type cells lead to a higher proliferative potential in the resulting dual-cadherin subclones (OvCa433Ncad+ and SKOV3Ecad+) relative to their parental cell lines. Additionally, being initially morphologically very distinct, both of these hybrid MCAs acquired very similar surface morphology upon acquisition of the second cadherin, indicative of cadherin regulation of MCA dynamics. Further, Ncad acquisition led to cell behaviors characteristic of a more aggressive phenotype including enhanced mesothelial adhesion, submesothelial migration, and invasion, suggesting a metastatic advantage for Ncad+ cells at the secondary site. This is consistent with immunohistochemical data of paired primary and metastatic tumors from the same patient showing enhanced Ncad expression in metastases [5]. In marked contrast, upregulation of Ecad resulted in less aggressive behavior as exhibited by attenuated adhesion to collagen matrices, mesothelial layers, and peritoneal explants. It is interesting to speculate that expression of Ecad may be more advantageous at the free-floating cell/MCA state, wherein it has been reported to promote resistance to anoikis and chemotherapy [30–33].

Previous studies have used a variety of approaches to measure the strength of Ecad:Ecad and Ncad:Ncad bonds. For example, a quantitative approach was designed to assess the intercellular adhesion strength of cadherins based on the measurement of the doublet separation force, the force required to separate a pair of cells connected for 0.5 to 30 minutes on one of the cell sides [62]. Results showed that Ecad:Ecad bonds are stronger than Ncad:Ncad

interactions. These data agree with results from a related study in which the authors performed single-molecule analysis of cadherin-mediated cell-cell adhesion, demonstrating that the rupture force of a single Ecad-Ecad bond is higher than that of a single Ncad-Ncad bond [63]. In the current study, we explored multicellular aggregation of cells at a concentration of approximately 2000 cells per aggregate and incubated them for 48 hours, allowing for unlimited cadherin bonding. Our observations show that mesenchymal-type cells (Ncad+) exhibit a distinct morphology in 3D clusters, wherein they stretch and spread over the entire surface of the cells already in the cluster. Thus, Ncad+ cells grown under MCA conditions contact neighboring cells using a much larger surface area than that seen either in two-dimensional cultures or with Ecad+ cells. In contrast, the epithelial-type cells (Ecad+) retain a more spherical shape that limits points of cell:cell contact to a much smaller surface area. Thus, although the force required to rupture a single bond or separate a single cell:cell pair may be larger for Ecad relative to Ncad, morphological distinctions unique to adhesive mechanisms adopted by cells in organotypic 3D culture systems appear to regulate overall aggregate adhesion and subsequent compaction.

In conclusion, our findings support the hypothesis that intraperitoneal MCA dynamics and ultimate metastatic success may be regulated by cadherin composition. Understanding the contribution of cadherin heterogeneity to intraperitoneal metastatic success is necessary for the development of targeted therapeutics tailored to address relevant biological processes in heterogeneous EOC tumors.

Supplementary data to this article can be found online at <http://dx.doi.org/10.1016/j.neo.2017.04.002>.

## Conflicts of Interest

The authors have no conflicts of interest to declare.

## Acknowledgements

This project was supported in part by National Institutes of Health Research Grants RO1CA109545 (M.S.S.) and RO1CA086984 (M.S.S.), the Leo and Anne Albert Charitable Trust (M.S.S.), Fulbright Foundation (Y.K.), the Research Like a Champion grant (Y.K., R.L.), and Notre Dame Integrated Imaging Facility. We thank Dr. Oleg Kim for providing technical assistance with statistical analysis.

## References

- [1] Siegel RL, Miller KD, and Jemal A (2015). Cancer statistics, 2015. *CA Cancer J Clin* **65**(1), 5–29.
- [2] Howlader N, Noone A, Krapcho M, Neyman N, Aminou R, Waldron W, Altekruse S, Kosary C, Ruhl J, Tatalovich Z, et al (2011). SEER cancer statistics review, 1975–2008. Bethesda, MD: National Cancer Institute; 2011 19.
- [3] Vaughan S, Coward JI, Bast RC, Berchuck A, Berek JS, Brenton JD, Coukos G, Crum CC, Drapkin R, Etemadmoghadam D, et al (2011). Rethinking ovarian cancer: recommendations for improving outcomes. *Nat Rev Cancer* **11**(10), 719–725.
- [4] Marcus CS, Maxwell GL, Darcy KM, Hamilton CA, and McGuire WP (2014). Current approaches and challenges in managing and monitoring treatment response in ovarian cancer. *J Cancer* **5**(1), 25.
- [5] Hudson LG, Zeineldin R, and Stack MS (2008). Phenotypic plasticity of neoplastic ovarian epithelium: unique cadherin profiles in tumor progression. *Clin Exp Metastasis* **25**(6), 643–655.
- [6] Lengyel E (2010). Ovarian cancer development and metastasis. *Am J Pathol* **177**(3), 1053–1064.
- [7] Pradeep S, Kim SW, Wu SY, Nishimura M, Chaluvally-Raghavan P, Miyake T, Pecot CV, Kim S, Choi HJ, Bischoff FZ, et al (2014). Hematogenous metastasis of ovarian cancer: rethinking mode of spread. *Cancer Cell* **26**(1), 77–91.

- [8] Coffman LG, Burgos-Ojeda D, Wu R, Cho K, Bai S, and Buckanovich RJ (2016). New models of hematogenous ovarian cancer metastasis demonstrate preferential spread to the ovary and a requirement for the ovary for abdominal dissemination. *Transl Res*.
- [9] Allen H, Porter C, Gamarra M, Piver M, and Johnson E (1987). Isolation and morphologic characterization of human ovarian carcinoma cell clusters present in effusions. *Pathobiology* **55**(4), 194–208.
- [10] Casey RC, Burleson KM, Skubitz KM, Pambuccian SE, Oegema TR, Ruff LE, and Skubitz AP (2001).  $\beta$ 1-integrins regulate the formation and adhesion of ovarian carcinoma multicellular spheroids. *Am J Pathol* **159**(6), 2071–2080.
- [11] Burleson KM, Casey RC, Skubitz KM, Pambuccian SE, Oegema Jr TR, and Skubitz APN (2004). Ovarian carcinoma ascites spheroids adhere to extracellular matrix components and mesothelial cell monolayers. *Gynecol Oncol* **93**(1), 170–181.
- [12] Burleson KM, Boente MP, Pambuccian SE, and Skubitz AP (2006). Disaggregation and invasion of ovarian carcinoma ascites spheroids. *J Transl Med* **4**, 6.
- [13] Friedrich J, Seidel C, Ebner R, and Kunz-Schughart LA (2009). Spheroid-based drug screen: considerations and practical approach. *Nat Protoc* **4**(3), 309–324.
- [14] Larson B, Slawny N, Luty W, and Banks P (2014). Targeting hypoxic tumor cells in 3D spheroids. *Genet Eng Biotechnol News Omics* **34**(16), 26.
- [15] Tung Y, Hsiao AY, Allen SG, Torisawa Y, Ho M, and Takayama S (2011). High-throughput 3D spheroid culture and drug testing using a 384 hanging drop array. *Analyst* **136**(3), 473–478.
- [16] He X, Chien J, and Shridhar V (2013). Assessment of resistance to anoikis in ovarian cancer. Ovarian cancer. Springer; 2013. p. 347–354.
- [17] Lee JM, Mhawech-Fauceglia P, Lee N, Parsanian LC, Lin YG, Gayther SA, and Lawrenson K (2013). A three-dimensional microenvironment alters protein expression and chemosensitivity of epithelial ovarian cancer cells in vitro. *Lab Invest* **93**(5), 528–542.
- [18] Weiswald L-B, Bellet D, and Dangles-Marie V (2015). Spherical cancer models in tumor biology. *Neoplasia* **17**(1), 1–15.
- [19] Friedrich J, Ebner R, and Kunz-Schughart LA (2007). Experimental anti-tumor therapy in 3-D: spheroids—old hat or new challenge? *Int J Radiat Biol* **83**(11–12), 849–871.
- [20] Guarino M, Rubino B, and Ballabio G (2007). The role of epithelial-mesenchymal transition in cancer pathology. *Pathology* **39**(3), 305–318.
- [21] Onder TT, Gupta PB, Mani SA, Yang J, Lander ES, and Weinberg RA (2008). Loss of E-cadherin promotes metastasis via multiple downstream transcriptional pathways. *Cancer Res* **68**(10), 3645–3654.
- [22] Weinberg R (2013). The biology of cancer. Garland Science; 2013.
- [23] Patel IS, Madan P, Getsios S, Bertrand MA, and MacCalman CD (2003). Cadherin switching in ovarian cancer progression. *Int J Cancer* **106**(2), 172–177.
- [24] Auersperg N, Wong AST, Choi K, Kang SK, and Leung PCK (2001). Ovarian surface epithelium: biology, endocrinology, and pathology. *Endocr Rev* **22**(2), 255–288 [2015/03].
- [25] Derycke LD and Bracke ME (2004). N-cadherin in the spotlight of cell-cell adhesion, differentiation, embryogenesis, invasion and signalling. *Int J Dev Biol* **48**, 463–476.
- [26] Ahmed N, Thompson EW, and Quinn MA (2007). Epithelial-mesenchymal interconversions in normal ovarian surface epithelium and ovarian carcinomas: an exception to the norm. *J Cell Physiol* **213**(3), 581–588.
- [27] Levanon K, Crum C, and Drapkin R (2008). New insights into the pathogenesis of serous ovarian cancer and its clinical impact. *J Clin Oncol* **26**(32), 5284–5293.
- [28] King SM, Hilliard TS, Wu LY, Jaffe RC, Fazleabas AT, and Burdette JE (2011). The impact of ovulation on fallopian tube epithelial cells: evaluating three hypotheses connecting ovulation and serous ovarian cancer. *Endocr Relat Cancer* **18**(5), 627–642.
- [29] Poncelet C, Cornelis F, Tepper M, Sauce E, Magan N, Wolf JP, and Ziolk M (2010). Expression of E- and N-cadherin and CD44 in endometrium and hydrosalpinges from infertile women. *Fertil Steril* **94**(7), 2909–2912.
- [30] Bates RC, Edwards NS, and Yates JD (2000). Spheroids and cell survival. *Crit Rev Oncol* **36**(2), 61–74.
- [31] Desoize B and Jardillier J (2000). Multicellular resistance: a paradigm for clinical resistance? *Crit Rev Oncol* **36**(2), 193–207.
- [32] Frankel A, Rosen K, Filmus J, and Kerbel RS (2001). Induction of anoikis and suppression of human ovarian tumor growth in vivo by down-regulation of Bcl-X(L). *Cancer Res* **61**(12), 4837–4841.
- [33] Green SK, Francia G, Isidoro C, and Kerbel RS (2004). Antiadhesive antibodies targeting E-cadherin sensitize multicellular tumor spheroids to chemotherapy in vitro. *Mol Cancer Ther* **3**(2), 149–159.
- [34] Reddy P, Liu L, Ren C, Lindgren P, Boman K, Shen Y, Lundin E, Ottander U, Rytinki M, Liu K, et al (2005). Formation of E-cadherin-mediated cell-cell adhesion activates AKT and mitogen activated protein kinase via phosphatidylinositol 3 kinase and ligand-independent activation of epidermal growth factor receptor in ovarian cancer cells. *Mol Endocrinol* **19**(10), 2564–2578.
- [35] Burkhalter RJ, Symowicz J, Hudson LG, Gottardi CJ, and Stack MS (2011). Integrin regulation of beta-catenin signaling in ovarian carcinoma. *J Biol Chem* **286**(26), 23467–23475.
- [36] Liu Y, Burkhalter R, Symowicz J, Chaffin K, Ellerbroek S, and Stack MS (2012). Lysophosphatidic acid disrupts junctional integrity and epithelial cohesion in ovarian cancer cells. *J Oncol* **2012**.
- [37] Wu C, Cipollone J, Maines-Bandiera S, Tan C, Karsan A, Auersperg N, and Roskelley CD (2008). The morphogenic function of E-cadherin-mediated adherens junctions in epithelial ovarian carcinoma formation and progression. *Differentiation* **76**(2), 193–205.
- [38] Kelm JM, Timmins NE, Brown CJ, Fussenegger M, and Nielsen LK (2003). Method for generation of homogeneous multicellular tumor spheroids applicable to a wide variety of cell types. *Biotechnol Bioeng* **83**(2), 173–180.
- [39] Matsuyoshi N, Toda K, and Imamura S (1998). N-cadherin expression in human adult T-cell leukemia cell line. *Arch Dermatol Res* **290**(4), 223–225.
- [40] Lengyel E, Burdette J, Kenny H, Matei D, Pilrose J, Haluska P, Nephew K, Hales D, and Stack MS (2014). Epithelial ovarian cancer experimental models. *Oncogene* **33**(28), 3619–3633.
- [41] Bruney L, Conley KC, Moss NM, Liu Y, and Stack MS (2014). Membrane-type I matrix metalloproteinase-dependent ectodomain shedding of mucin16/CA-125 on ovarian cancer cells modulates adhesion and invasion of peritoneal mesothelium. *Biol Chem* **395**(10), 1221–1231.
- [42] Sodek KL, Ringuette MJ, and Brown TJ (2009). Compact spheroid formation by ovarian cancer cells is associated with contractile behavior and an invasive phenotype. *Int J Cancer* **124**(9), 2060–2070.
- [43] Sivertsen S, Berner A, Michael CW, Bedrossian C, and Davidson B (2006). Cadherin expression in ovarian carcinoma and malignant mesothelioma cell effusions. *Acta Cytol* **50**(6), 603.
- [44] Gavard J, Lambert M, Grosheva I, Marthiens V, Irinopoulou T, Riou JF, Bershady A, and Mege RM (2004). Lamellipodium extension and cadherin adhesion: two cell responses to cadherin activation relying on distinct signalling pathways. *J Cell Sci* **117**(Pt 2), 257–270.
- [45] Machesky LM (2008). Lamellipodia and filopodia in metastasis and invasion. *FEBS Lett* **582**(14), 2102–2111.
- [46] Hegedüs B, Marga F, Jakab K, Sharpe-Timms KL, and Forgacs G (2006). The interplay of cell-cell and cell-matrix interactions in the invasive properties of brain tumors. *Biophys J* **91**(7), 2708–2716.
- [47] Townes PL and Holtfreter J (1955). Directed movements and selective adhesion of embryonic amphibian cells. *J Exp Zool* **128**(1), 53–120.
- [48] Steinberg MS and Gilbert SF (2004). Townes and Holtfreter (1955): directed movements and selective adhesion of embryonic amphibian cells. *J Exp Zool A Comp Exp Biol* **301A**(9), 701–706.
- [49] Foty RA and Steinberg MS (2005). The differential adhesion hypothesis: a direct evaluation. *Dev Biol* **278**(1), 255–263.
- [50] Merks RM and Glazier JA (2005). A cell-centered approach to developmental biology. *Physica A* **352**(1), 113–130.
- [51] Armstrong NJ, Painter KJ, and Sherratt JA (2006). A continuum approach to modelling cell-cell adhesion. *J Theor Biol* **243**(1), 98–113.
- [52] Straub BK, Rickett S, Zimbelmann R, Grund C, Kuhn C, Iken M, Ott M, Schirmacher P, and Franke WW (2011). E-N-cadherin heterodimers define novel adherens junctions connecting endoderm-derived cells. *J Cell Biol* **195**(5), 873–887.
- [53] Carey SP, Starchenko A, McGregor AL, and Reinhart-King CA (2013). Leading malignant cells initiate collective epithelial cell invasion in a three-dimensional heterotypic tumor spheroid model. *Clin Exp Metastasis* **30**(5), 615–630.
- [54] Jolly MK, Boareto M, Huang B, Jia D, Lu M, Ben-Jacob E, Onuchic JN, and Levine H (2015). Implications of the hybrid epithelial/mesenchymal phenotype in metastasis. *Front Oncol* **5**.
- [55] Chao Y, Wu Q, Acquafondata M, Dhir R, and Wells A (2012). Partial mesenchymal to epithelial reverting transition in breast and prostate cancer metastases. *Cancer Microenviron* **5**(1), 19–28.
- [56] Hecht I, Bar-El Y, Balmer F, Natan S, Tsarfay I, Schweitzer F, and Ben-Jacob E (2015). Tumor invasion optimization by mesenchymal-amoebooid heterogeneity. *Sci Rep* **5**.
- [57] Friedl P and Wolf K (2010). Plasticity of cell migration: a multiscale tuning model. *J Cell Biol* **188**(1), 11–19.
- [58] Bastos LG, de Marcondes PG, de-Freitas-Junior JC, Leve F, de Souza WF, de Araujo WM, Tanaka MN, Abdelhay ES, and Morgado-Diaz JA (2014). Progeny

- from irradiated colorectal cancer cells acquire an EMT-like phenotype and activate Wnt/ $\beta$ -catenin pathway. *J Cell Biochem* **115**(12), 2175–2187.
- [59] Hiscox S, Jiang WG, Obermeier K, Taylor K, Morgan L, Burmi R, Barrow D, and Nicholson RI (2006). Tamoxifen resistance in MCF7 cells promotes EMT-like behaviour and involves modulation of  $\beta$ -catenin phosphorylation. *Int J Cancer* **118**(2), 290–301.
- [60] Wu Y, Ginther C, Kim J, Mosher N, Chung S, Slamon D, and Vадgama JV (2012). Expression of Wnt3 activates Wnt/ $\beta$ -catenin pathway and promotes EMT-like phenotype in trastuzumab-resistant HER2-overexpressing breast cancer cells. *Mol Cancer Res* **10**(12), 1597–1606.
- [61] Strauss R, Li Z, Liu Y, Beyer I, Persson J, Sova P, Moller T, Pesonen S, Hemminki A, Hamerlik P, et al (2011). Analysis of epithelial and mesenchymal markers in ovarian cancer reveals phenotypic heterogeneity and plasticity. *PLoS One* **6**(1), e16186.
- [62] Chu YS, Thomas WA, Eder O, Pincet F, Perez E, Thiery JP, and Durour S (2004). Force measurements in E-cadherin-mediated cell doublets reveal rapid adhesion strengthened by actin cytoskeleton remodeling through Rac and Cdc42. *J Cell Biol* **167**(6), 1183–1194.
- [63] Panorchan P, Thompson MS, Davis KJ, Tseng Y, Konstantopoulos K, and Wirtz D (2006). Single-molecule analysis of cadherin-mediated cell-cell adhesion. *J Cell Sci* **119**(Pt 1), 66–74.